SELF-HEALING PROCESSES IN COIL COATED CLADDING STUDIED BY THE SCANNING VIBRATING ELECTRODE

R.M. Souto[1], B. Normand[2,†], H. Takenouti[2] and M. Keddam[2]

[1] *Department of Physical Chemistry, University of La Laguna, E-38200 La Laguna (Tenerife), Canary Islands, Spain*

[2] *Laboratory of Interfaces and Electrochemical Systems, University Pierre and Marie Curie, C.P. 133, 4 place Jussieu, 75252 Paris Cedex, France*

[†] *Current address: Laboratory of Industrial Physicochemistry, INSA, Bât Léonard de Vinci, 21 Av. Jean Capelle, 69621 Villeurbanne Cedex, France*

ABSTRACT

The ability of the zinc layer in coil-coated cladding to protect the underlying metal substrate exposed to the environment through a sub-centimetre circular defect was established by using the scanning vibrating electrode technique (SVET). The onset of electrochemical corrosion is observed through the development of local anodes and cathodes in the defective system, with the formation of soluble zinc species. The dissolution process is maintained until a sufficiently high concentration is attained by the metal ions, and their subsequent precipitation inside the holiday blocks the defect as to hinder further corrosion. A self healing effect was thus observed. The role of zinc salts was confirmed by SEM and EDX observations.

Key words: Defective organic coating, Self-healing effect, Local current density, Scanning vibrating electrode technique, Coil-coated steel.

1. INTRODUCTION

Coil-coated cladding is a widely used roofing and siding material. It is typically organically-coated galvanised steel, with additional protection provided by an organic coating and top coat. Importantly, the primer contains corrosion inhibitor pigments, whose effectiveness rely on their removal from the primer coating into a corrosion solution and transport to the bare surfaces. Profile and panel manufacturers roll-form the coil-coated strip-steel and guillotine it into shorter lengths for installation. The cutting operation produces bare (uncoated) edges of steel and zinc which are directly exposed to the atmosphere. Subsequent galvanic corrosion of the steel (cathode) and zinc (anode) occurs at the cut-edge and results in the recession of the zinc coating and consequent loss of the interface between the organic coating and the cut-edge [1-3]. This eventually leads to unsightly peelback of the organic coating and the development of red rust on the steel at the cut-edge [1,2]. In addition, mechanical damage to the coating may often take place either during transportation or construction, typically from foot traffic on roofs, incorrect fixing and joining practice, and careless installation.

The mechanisms of the corrosion processes that take place in the vicinity of defects are not yet completely known. Conventional electrochemical techniques, including electrochemical impedance spectroscopy (EIS), are integral methods and thus lack spatial resolution, which is a major drawback specially in the case of defective coated metals. Therefore, localized electrochemical techniques with spatial resolution in the micro and submicrometric ranges are becoming increasingly used in the corrosion laboratory for the study of these systems. At present, interesting new information concerning the electrochemical and degradation processes at defective coated metals is being obtained with the scanning vibrating electrode technique (SVET) [4-19], the scanning Kelvin-probe (SKP) [20-30], localized electrochemical impedance spectroscopy (LEIS) [12,13,31-38], and scanning electrochemical microscopy [39-49].

In this paper we present the results of an investigation specially directed to explore the applicability of the scanning vibrating electrode technique (SVET) to the electrochemical processes related to galvanic corrosion and self-healing originating from a defect in an organic coating on a metal. Experimental observations were conducted on coil-coated architectural cladding which consists of mild steel covered by a metallic layer of a Zn alloy and then coated with a polyester resin. A holiday was created in the coating to reach the underlying steel substrate, and subsequently immersed in 3% NaCl solution. The ability of the zinc layer to protect the defect through its dissolution and eventual blockage of the defect by precipitation of corrosion products could be thus investigated.

2. EXPERIMENTAL

Experiments were carried out on a coil-coating steel. It consisted of a steel sheet 400 μm thick, covered with a zinc-containing metallic layer of 20 μm thickness, a pre-treatment consisting of chromate and the paint. The composition of the intermediate zinc-based metallic coating was Zn-5% Al alloy (Galfan, *Zn-5Al*). The paint system consisted of a 5 μm polyester primer containing strontium chromate as inhibitor, which was also covered with a 20 μm polyester topcoat containing titanium dioxide as filler. Samples of 50 mm x 50 mm were cut from the coil-coated steel panels with a guillotine.

A 1.0 mm diameter conical holiday was produced in the polyester coating by means of a drill such that the underlying carbon steel surface was exposed. Exposure of the galvanized intermediate layer to the electrolyte also occurred at the conical lateral sides of the holiday. Figure 1 shows schematically the drilling of the coated specimen. A photograph of the resulting surface performed with an optical microscope is shown in figure 2.

The corrosion test cells were then created by adhering a PMMA-built circular cell (Ø=3.5 cm), in which a 10 mm x 10 mm opening was produced in the bottom, to the polyester surface of the coil-coated steel sample, such that the artificial holiday was in the centre. Adhesion was achieved by the sparing use of silicone sealant (Silastic 732 RTV). The corrosion test medium was 3 wt-% NaCl aqueous solution. The electrolyte covered the specimen under investigation by ca. 3 mm. All experiments were performed at ambient temperature in the naturally aerated cell. No polarization was applied to the samples, which were at their corresponding open circuit potential.

The local current density was determined with a SVET device from Applicable Electronics (USA), by scanning the vibrating electrode over the specimen at a height of 30 μm. This device causes the vibrating probe to simultaneously oscillate in two directions, namely perpendicular to the surface (*Z*-axis) and another parallel to the surface. In this study, the probe was set to oscillate in the *X*-axis, that is, in the same direction the probe position moved along the line scans. The electrode was set to vibrate at 203 Hz in the *Z* direction and at 512 Hz in the *X* direction. A video camera connected to an optical microscope was introduced in the system to follow the movement of the vibrating electrode over the sample during operation. The vibrating probe was a thin Pt needle covered with parylène® and leaving the metal exposed only at the needle's tip, on which a platinum black sphere of ca. 20 μm in diameter was deposited.

3. RESULTS AND DISCUSSION

Testing of the samples with SVET technique was carried out on the coated surfaces with an artificial defect immediately following their immersion in the test solution. The development of electrochemical activity in and around the holiday could be monitored by recording the current densities flowing in the solution. In this study, line scans passing approximately over the diameter of the holiday were carried out by shifting the vibrating probe at constant height over the sample. The movement of the probe was performed in 800 steps in the *X*-axis, and the step distance between collections was 2 μm, thus the total travel distance covered in each line scan amounted 1.6 mm along the *X* direction.

A typical plot for the global current measured at the probe is shown in figure 3A. From this figure, it can be seen that finite current densities were measured when the microelectrode passed over the hole. This figure displays the vectors that result from the combination of *Z* and *X* contributions to the probe current. The position of the end of the vector can be observed to describe varying angles in relation to the *Z*-axis (i.e., the vertical axis in this figure) as the probe is shifted from left to right to perform a line scan over the holiday. In all cases, current density vectors account for the release of ionic species from the reactive surface exposed to the electrolyte inside the holiday, though they can effectively correspond to either cations (namely soluble metal species) when the vibrating probe passes over an anodic region, or to anions (i.e. hydroxyl ions as the end product for oxygen electroreduction) when the tip scans a cathodic region instead. The different sign of the charge carried by anions and cations can be distinguished in the figure by considering the direction of the *Z*-component of the current density vectors, which would be directed towards and outwards the active surface, respectively. The sign convention employed implies that positive current density values will correspond to a flow of cations leaving the corroding surface, whereas the negative values to a flow of anions departing from the sample. On the other hand, regardless the sign of the current vectors along the *Z*-axis, the position of their ends can be found to either turn to the left or to the right in the image, respectively opposing or following the scan direction during the measurement. Therefore, the *X*-component of the vectors describes how fast the ionic fluxes leaving the surface divert from the vertical direction to advance laterally in the electrolyte phase over the intact coating. This is the reason that a purely vertical vector facing upwards in the plot could be observed only when the vibrating probe was located exactly where the maximum anodic activity occurs. Though the exposed zinc is located in a circle surrounding the steel at the center of the holiday, anodic activity was only observed at the left side of the scan line. This result did not come as a surprise because it is well known that the distribution of anodic sites over zinc samples exposed to a chloride-containing electrolyte often starts at quite reduced areas from the onset of pitting [13,50]. On the other hand, the

cathodic activity is observed at the right side of the scan line depicted in figure 3A, and it is distributed over all the exposed steel surface, which is the usual observation for Zn-Fe galvanic coupling in chloride environments for both the uncoated metals when electrically connected [50], and at cut edges in coated galvanized steel [13].

Additionally, it must be noticed that a ghost needle is also seen in figure 3A, which is displayed in the upper part of the photograph. It is originated by a mirror that was placed behind the cell to allow a more accurate positioning of the SVET probe from the electrode surface. In this ghost image, the SVET vibration is not seen, and thus a sharp needle is depicted. It is also worth to notice that the needle was located perpendicular to the scan-direction to monitor the *X*-axis component.

The vertical component of the current density values (i.e., along *Z*-axis) measured during the line scan depicted in figure 3A could be plotted both as vectors (the corresponding graph is depicted in figure 3B superimposed above the optical image of the defect), and quantitatively as a function of displacement as displayed in figure 4. From the inspection of the latter graph, it can be observed that non-zero currents were measured when the vibrating electrode passed above the circular defect, and that both positive and negative values were measured along a line scan. But it was also observed from figure 4 that neither the maximum of the positive current peak nor the point at which the zero current was measured occurred at the geometrical centre of the defect. Though the positive current peak lies around 100 μm to the left of the holiday's centre, the zero current point was found at ca. 45 μm to the right side. Furthermore, the observed shift was found to be independent of the scan direction, as discovered by immediately recording a second line scan after reversal of the scan direction (also given in figure 4). Thus, a geometrical calibration of the system was required prior to relating the measured currents to specific locations over the scanned sample.

Calibration of the system was performed by imposing a –60 nA current to the system from a second Pt needle which acted as a point current source because only the metal at the needle's tip was exposed. The vibrating probe was located 50 μm above the current source, and the local current density was subsequently measured. Figure 5 displays both the theoretical local current density for the *Z*-direction and the experimental data as recorded during this experiment. It is clearly observed that a shift of 44.5 μm existed between the current signal measured at the microelectrode and the theoretical value based on the image recorded by the video-microscope. Thus, it was concluded that the 45 μm shift found in figure 4 was exclusively an instrumental artefact, and the zero current value for $j(Z)_{loc}$ actually occurred at the centre of the drilled hole.

The time course of the corrosion processes at the defect was then followed by recording the local current during consecutive line scans whereas the sample was immersed in the test solution.

The measured line scans over the holiday for various exposures are depicted in figures 6 and 7, which correspond to the situations when the electrode was vibrating parallel (*X*-axis) and perpendicular (*Z*-axis) to the scan direction, respectively, whereas the corresponding scalar products of the two current densities are shown in figure 8. The current density was about five times greater in the *Z* direction than in the *X* direction. That is, the ionic current flowing perpendicular to the surface is significantly bigger than that flowing parallel to it. The holiday can thus be regarded as a source of metal ions that diffuse in the electrolyte mainly departing from the surface when measured with the probe vibrating at a constant height of 30 μm relative to the surrounding coated surface, whereas this ionic flux widens over the coating at a smaller rate. Furthermore, the anodic activity is located at about 100 μm from the centre of the holiday (cf. figure 8).

As time elapsed, a continuous increase of the current measured over the defect was found during the earlier hours of immersion. Electrochemical activity developed within the uncoated area as a result of the establishment of a galvanic cell inside the holiday. Figure 9 depicts the time variation of the peak current density for the graphs presented in figure 8. Since no experiments could be carried out during the night, there is a major time-lapse between data collections. However, the time course of the current density could be tentatively estimated in this figure by interpolation. Thus, a marked decrease of the local current density could be expected after six hours exposure.

It was also observed that the peak position in the total current density plots shifted with time. The shift of peak position observed from the components related to the vibration in both *Z* and *X* directions is thus plotted in figure 10 respective to the centre of the holiday. This figure illustrates clearly that the peak position shifted towards the left with time. From the value of the maximum current density observed in figure, which is less than 1 mA cm^{-2}, and by applying the Faraday law, it could be estimated that less than 1.5 μm of the Zn coating was dissolved within one hour. Compared with the thickness of zinc coating, equal to 20 μm, this shift of the current peak is not due to the exhausting of the zinc layer, but rather to the formation of zinc corrosion products that decrease the reactivity of the electrode surface.

The line scan showed clearly the cathodic zone in the right and the anodic zone at the left of the artificial defect. This effect is more clearly illustrated by considering the complete current density maps measured over the holiday. Figure 11 shows the contour curve and the 3-D representation of the current density distribution when the probe was vibrated in the *Z*-direction above the drilled hole as measured after the previously-described sequence of experiments was completed (i.e, 20 hours after the specimen was immersed in the test electrolyte). The electrode half-reactions are greatly localized as it could be expected from the previous line-scan experiments. At the centre of the hole,

the current density flowing in the *Z* direction is almost zero, whereas the anodic area is located about 140 μm (without taking account of the experimental artefact of the probe position) to the left from the centre of the drilled hole as illustrated in Figure 9. On the other hand, the cathodic peak is located about 200 μm from the centre of the hole.

The reported distribution originates from the drilling procedure used to produce the defect in the coating. The base steel matrix was reached at the bottom of the hole, whereas the zinc-containing galvanized layer was left exposed at the conical-shaped border sides of the defect, as depicted in figure 1. The anodic peak is likely due to the anodic dissolution of zinc:

$$Zn \rightarrow Zn^{2+} + 2\ e^{-}$$

This zinc cation will form zinc hydroxy-chloride species, $Zn_5(OH)_8Cl_2$ and $Zn(OH)_2$ [51,52], which are less soluble and precipitate around it. This process is the main effect of self healing effect of the zinc coated steel. The cathodic reaction taking place at the right in the defect area is likely to be the reduction of dissolved oxygen naturally occurring in the aerated electrolyte.

At longer exposure times a major decrease of the electrochemical activity in the defect is then observed. This originates from the precipitation of corrosion products within the holiday, which effectively block the sites where the cathodic half-cell reaction was observed to occur. In this way, the corrosion rate is significantly diminished, and the onset of a self-healing process is found. Figure 12 presents the SEM picture and the EDX-distribution of some elements around the drilled hole. The concentrations of chlorine and zinc are high at the centre where the steel was exposed. The formation of the zinc – chloride salt is therefore verified. Aluminum is enriched around the steel exposed area. This element will be transformed in alumina and remained around it. Chromium, used for the surface pre-treatment before application of the organic coating is also detected by EDX analyses, and a possible additional effect towards self-healing of the defective coating due to the action of chromate ions could not be discarded at this stage.

From the foregoing, it has been demonstrated that valuable information concerning the corrosion processes at defective coated samples could be extracted by using the scanning vibrating electrode technique over a sample that is not flat provided the vibrating probe is scanned at a close distance from the surface. In order to establish the operating height for the experiments, a number of considerations needed special attention. Firstly, the scanning probe is submitted to mechanical movement, thus care must be taken that the tip will not touch the sample during operation. Next, some additional distance must be provided that convective effects imposed to the electrolyte by the vibrating probe would not disturb the current distributions near the surface. In this way, considering the sizes of both the platinum black sphere and the amplitude of vibration along the *Z*-axis, a height

of 30 μm over the intact coating surrounding the holiday was adopted throughout. Under these conditions, the maximum distance between the tip and the sample would be established at the centre of the holiday, over the steel matrix, amounting to about 75 μm, a value considerably smaller than the typical distances employed to scan flat surfaces in previous investigations with the SVET [13].

Another feature to be highlighted from this work is that high resolution measurements were conducted for a sample that was not flat. That is, the defect was operated through the coating to expose the underlying metal layers without sleeving the sample in a holder at both coated sides, which is the typical procedure employed in previous investigations at cut edges [7,9,10,13]. With sleeved samples, the coating surface is not directly exposed to the test environment apart from the cut edge, nor the olymer matrix can swell as result of the corrosion reaction leading to delamination. Additionally, no volume is left for an aggressive electrolyte to be developed in direct contact to the bare exposed metal when the sample is flat, though it is well known that many localized corrosion processes, including blistering, have been observed to strongly depend on the composition of the restricted environment directly resulting from either one or both corrosion half-cell reactions. All these limitations have been overcome by drilling a hole directly through the coating for a sample facing upwards to the electrolyte, and by employing the proposed configuration further insights on delamination and self-healing processes should be gained in the near future.

Finally, an interesting outcome of our experiments is that both the spatial resolution and the operating distance employed for SVET is comparable with those already achieved by employing scanning electrochemical microscopy (SECM) for the same experimental system [41]. This will allow the same samples to be investigated with both techniques and combined data to be gathered on the electrochemical system.

4. CONCLUSIONS

This work has demonstrated the usefulness of the scanning vibrating electrode technique in characterizing *in situ* the electrochemical activity in the proximity of a sub-centimeter defect (holiday) through a polymeric coating applied on coil cladding steel during immersion in aqueous chloride solution. The applicability of the scanning vibrating electrode technique (SVET) to the study of the electrochemical processes related to galvanic corrosion and self-healing occurring in a defect were explored. The spatial and electrochemical resolutions of the technique were found to be very adequate to the study of the proposed corrosion system when the vibrating tip was scanned at a constant height of 30 μm.

Testing of the samples with the SVET technique was carried out on the coated surfaces with an artificial defect immediately following their immersion in the test solution. The development of electrochemical activity in and around the holiday could be monitored by recording the current densities flowing in the solution when the vibrating electrode was rastered over it. The signals recorded by scanning the specimen allowed the detection of the anodic and cathodic reaction sites to be performed, as well as to deduce the electrochemical reactions involved.

The current signals recorded by SVET were observed to greatly vary as time elapsed, and two different behaviours can be deduced from our data. Initially, the total current densities measured over the holiday show a steady increase with time following immersion of the specimen in the test environment, which resulted in the electrochemical activation of the defect as a result of the direct exposure of the underlying metal substrate to the electrolytic solution. Secondly, at times long enough, a major decrease in the current densities flowing from the holiday were observed as a self-healing process occurred from the precipitation of zinc-containing salts. The sacrificial effect of zinc for steel protection is effective for a circular defect in the polymeric paint with dia. 0.5 mm.

Acknowledgements:

We gratefully acknowledge the financial support of this work by the Ministerio de Educación y Ciencia (Madrid, Spain) in the framework of Project BQU2000-0864, CTQ2005-06446/BQU and CTQ2009-12459. This work was initiated within the framework of a Collaborative Research Programme funded by the Ministerio de Educación y Ciencia (Acción Integrada No. HF2001-003) between Spain and France.

References:

1. R.L. Howard, S.B. Lyon, J.D. Scantlebury, *Prog. Org. Coat.*, **37** (1999) 91.
2. R.L. Howard, S.B. Lyon, J.D. Scantlebury, *Prog. Org. Coat.*, **37** (1999) 99.
3. R.M. Souto, J.D. Scantlebury, *Prog. Org. Coat.*, **53** (2005) 63.
4. H. Isaacs, A.J. Aldykiewicz Jr., D. Thierry, T.C. Simpson, *Corrosion*, **52** (1996) 163.
5. D.A. Worsley, H.N. McMurray, A. Belghazi, *Chem. Commun.*, (1997) 2369.
6. F. Zou, C. Barreau, R. Hellouin, D. Quantin, D. Thierry, *Mater. Sci. Forum*, **289-292** (1998) 83.
7. K. Ogle, V. Baudu, L. Garrigues, X. Philippe, *J. Electrochem. Soc.*, **147** (2000) 3654.
8. J. He, V.J. Gelling, D.E. Tallman, G.P. Bierwagen, *J. Electrochem. Soc.*, **147** (2000) 3661.
9. D.A. Worsley, D. Williams, J.S.G. Ling, *Corros. Sci.*, **43** (2001) 2335.
10. D.A. Worsley, H.N. McMurray, J.H. Sullivan, I.P. Williams, *J. Electrochem. Soc.*, **149** (2002) B154.

11. T. Dung Nguyen, T. Anh Nguyen, M.C. Pham, B. Piro, B. Normand, H. Takenouti, *J. Electroanal. Chem.*, **572** (2004) 225.
12. I.M. Zin, S.B. Lyon, A. Hussain, *Prog. Org. Coat.*, **52** (2005) 126.
13. K. Ogle, S. Morel, D. Jacquet, *J. Electrochem. Soc.*, **153** (2006) B1.
14. D.J. Penney, J.H. Sullivan, D.A. Worsley, *Corros. Sci.*, **49** (2007) 1321.
15. G. Bierwagen, D. Battocchi, A. Simões, A. Stamness, D. Tallman, *Prog. Org. Coat.*, **59** (2007) 172.
16. M.L. Zheludkevich, K.A. Yasaku, A.C. Bastos, O.V. Karavai, M.G.S. Ferreira, *Electrochem. Commun*., **9** (2007) 2622.
17. F. Thébault, B. Vuillemin, R. Oltra, K. Ogle, C. Allely, *Electrochim. Acta*, **53** (2008) 5226.
18. S.V. Lamaka, M.L. Zheludkevich, K.A. Yasakau, R. Serra, S.K. Poznyak, M.G.S. Ferreira, *Prog. Org. Coat.*, **58** (2007) 127.
19. A.M. Simões, J. Torres, R. Picciochi, J.C.S. Fernandes, *Electrochim. Acta*, **54** (2009) 3857.
20. M. Stratmann, M. Wolpers, H. Streckel, R. Feser, *Ber. Bunsenges. Phys. Chem.*, **95** (1991) 1365.
21. A. Leng, H. Streckel, M. Stratmann, *Corros. Sci.*, **41** (1999) 547, 599.
22. M. Rohwerder, E. Hornung, M. Stratmann, *Electrochim. Acta*, **48** (2003) 1235.
23. B. Reddy, M.J. Doherty, J.M. Sykes, *Electrochim. Acta*, **49** (2004) 2965.
24. B. Reddy, J.M. Sykes, *Prog. Org. Coat.*, **52** (2005) 280.
25. R.J. Holness, G. Williams, D.A. Worsley, H.N. McMurray, *J. Electrochem. Soc.*, **152** (2005) B73.
26. G. Grundmeier, B. Rossenbeck, K.J. Roschmann, P. Ebbinghaus, M. Stratmann, *Corros. Sci.*, **48** (2006) 3716.
27. G. Klimow, N. Fink, G. Grundmeier, *Electrochim. Acta*, **53** (2007) 1290.
28. J.M. Sykes, M. Doherty, *Corros. Sci.*, **50** (2008) 2773.
29. A. Nazarov, T. Prosek, D. Thierry, *Electrochim. Acta*, **53** (2008) 7531.
30. M. Rohwerder, S. Isik-Uppenkamp, M. Stratmann, *Electrochim. Acta*, **54** (2009) 6058.
31. E. Bayet, F. Huet, M. Keddam, K.M. Ogle, H. Takenouti, *J. Electrochem. Soc.*, **144** (1997) 87.
32. F. Zou, D. Thierry, *J. Electrochem. Soc.*, 146 (1999) 2940.
33. L.V.S. Philippe, G.W. Walter, S.B. Lyon, *J. Electrochem. Soc.*, **150** (2003) B111.
34. T.D. Nguyen, M. Keddam, H. Takenouti, *Electrochem. Solid State Lett.*, **6** (2003) B25.
35. J.-B. Jorcin, E. Aragon, C. Merlatti, N. Pébère, *Corros. Sci.*, **48** (2006) 1779.
36. T.T.X. Hang, T.A. Truc, T.H. Nam, J.-B. Jorcin, N. Pébère, *Surf. Coat. Technol.*, **201** (2007) 7408.
37. C. Zhong, X.Tang, Y.F. Cheng, *Electrochim. Acta*, **53** (2008) 4740.

38. C.F. Dong, A.Q. Fu, X.G. Li, Y.F. Cheng, *Electrochim. Acta*, **54** (2008) 628.
39. R.M. Souto, Y. González-García, S. González, G.T. Burstein, *Corros. Sci.*, **46** (2004) 2621.
40. A.C. Bastos, A.M. Simões, S. González, Y. González-García, R.M. Souto, *Prog. Org. Coat.*, **53** (2005) 177.
41. R.M. Souto, Y. González-García, S. González, *Corros. Sci.*, **47** (2005) 3312.
42. K. Eckhard, T. Erichsen, M. Stratmann, W. Schuhmann, *Chem. Eur. J.*, **14** (2008) 3968.
43. A. Simões, D. Battocchi, D. Tallman, G. Bierwagen, *Prog. Org. Coat.*, **63** (2008) 260.
44. R.M. Souto, Y. González-García, S. González, *Corros. Sci.*, **50** (2008) 1638.
45. R.M. Souto, Y. González-García, S. González, G.T. Burstein, *Electroanalysis*, **21** (2009) 2569.
46. Y. Shao, C. Jia, G. Meng, T. Zhang, F. Wang, *Corros. Sci.*, **51** (2009) 371.
47. R.M. Souto, Y. González-García, S. González, *Prog. Org. Coat.*, **65** (2009) 435.
48. R.M. Souto, L. Fernández-Mérida, S. González, *Electroanalysis*, **21** (2009) 2640.
49. R.M. Souto, Y. González-García, J. Izquierdo, S. González, *Corros. Sci.*, **52** (2010) 548.
50. R.M. Souto, Y. González-García, A.C. Bastos, A.M. Simões, *Corros. Sci.*, **49** (2007) 4568.
51. M.C. Bernard, A. Hugot-le Goff, D. Massinon, N. Phillips, *Corros. Sci.*, **35** (1993) 1339.
52. A. Hugot-le Goff, M.C. Bernard, N. Phillips, *J. Electrochem. Soc.*, **142** (1995) 2162.

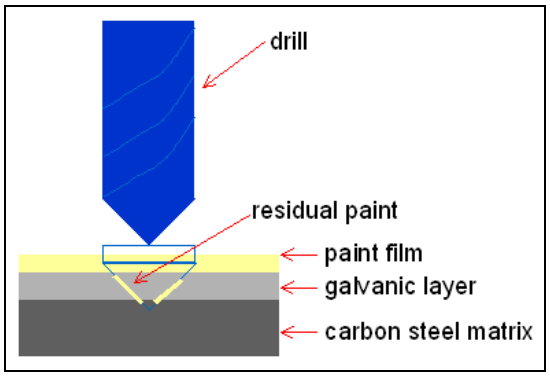

Figure 1: Schematics of the defect operated in the coating system.

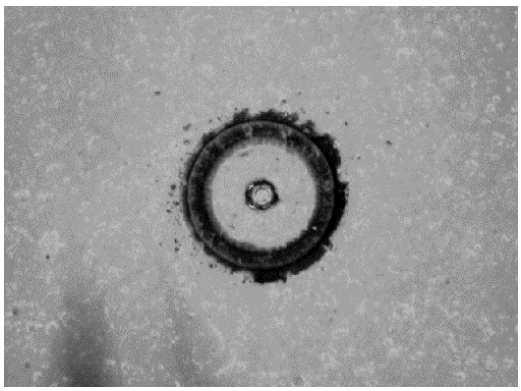

Figure 2: Optical image of defect operated in the coil-coated steel specimen with a drill.

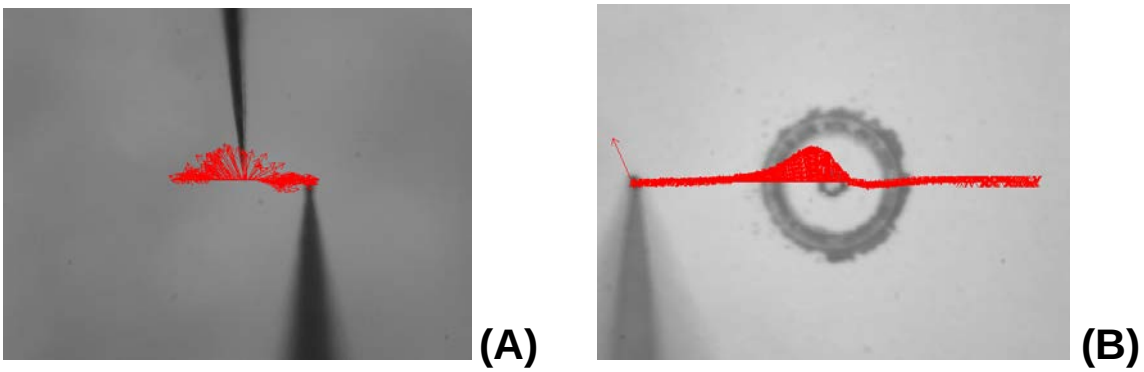

Figure 3: Line scan showing the electrochemical activity over the holiday as observed from (A) the measurement of the global current density $j(tot)_{loc}$, and (B) the corresponding vertical component of the current $j(Z)_{loc}$, for a sample immersed during 140 min in 3 wt% NaCl aqueous solution. Measurements at each point are displayed as vectors.

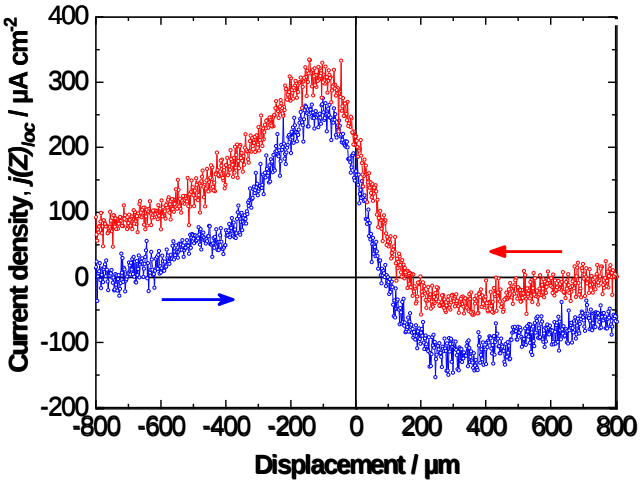

Figure 4: Effect of scan direction on the output signal for the vertical component of the current $j(Z)_{loc}$. Arrows indicate the scan direction for each line scan.

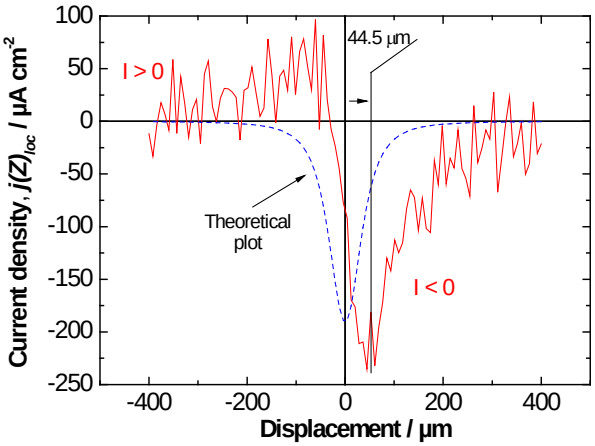

Figure 5: Calibration of the SVET system: Comparison of the experimental data with the theoretical plot for a point current source.

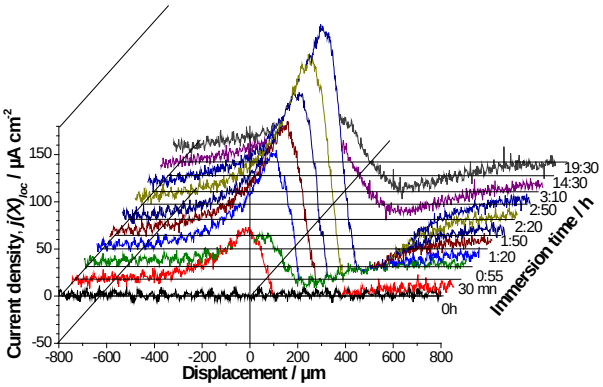

Figure 6: Variations in the local current measured above the holiday when the probe vibrates in the *X* direction, $j(X)_{loc}$, for various exposure times.

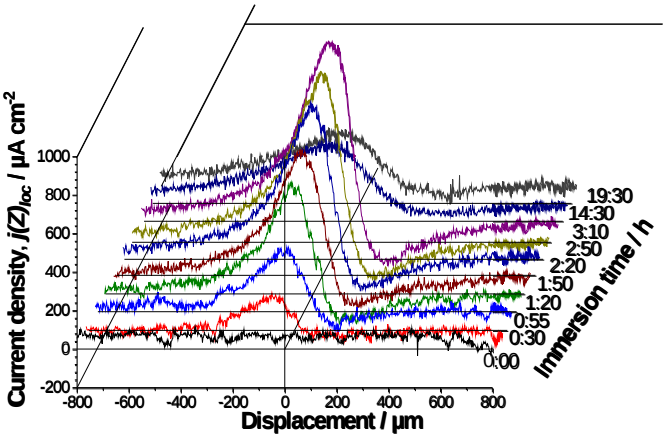

Figure 7: Variations in the local current measured above the holiday when the probe vibrates in the *Z* direction, $j(Z)_{loc}$, for various exposure times.

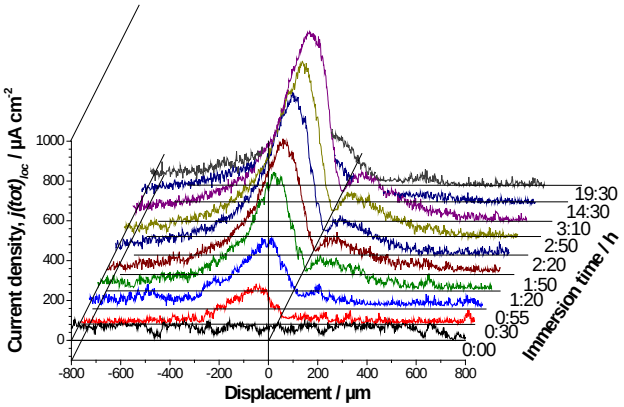

Figure 8: Variations in the total current, $j(tot)_{loc}$, measured above the holiday. Anodic activity is positive and cathodic activity is negative.

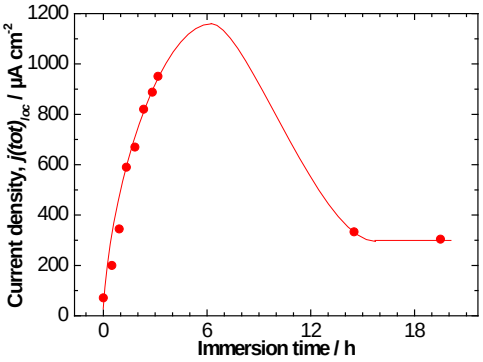

Figure 9: Time course of the current density values measured at the maxima of the plots given in figure 8, which correspond to the total current density determined from line scans measured over the centre of the holiday.

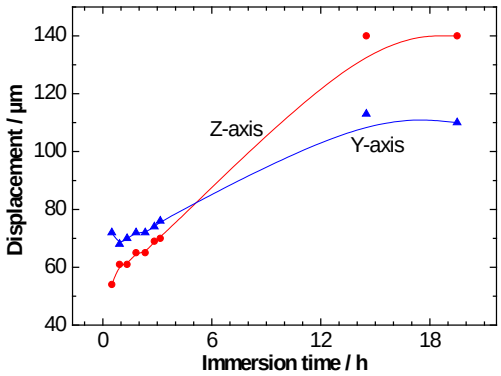

Figure 10: Time course for the shift in the position of the anodic peak observed for the parallel (*X*-axis) and (*Z*-axis) components of the ionic current density plots determined by SVET.

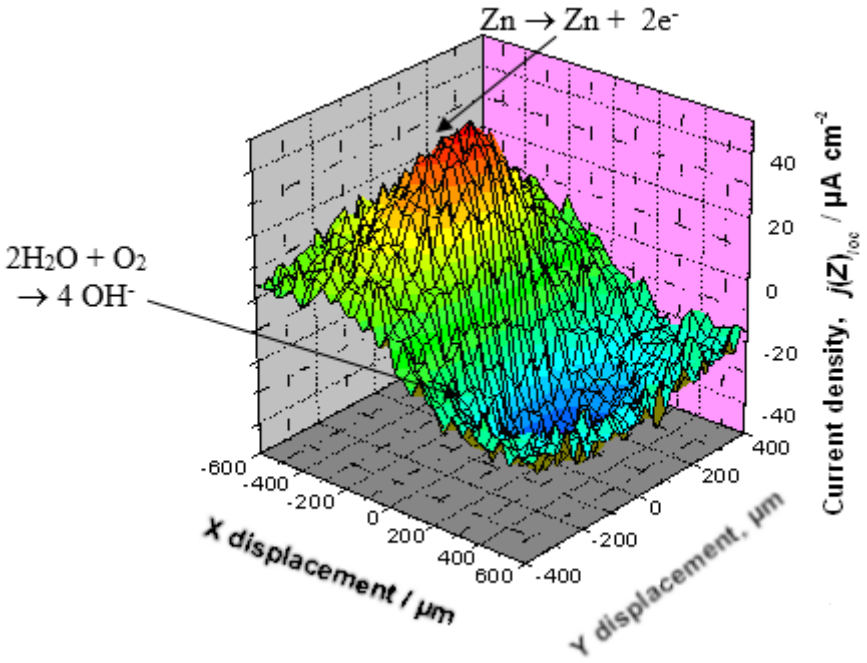

Figure 11: 3D representation of the *Z* component of the current density for the coil-coated sample with a circular defect after 20 h exposure to 3 wt% NaCl aqueous solution.

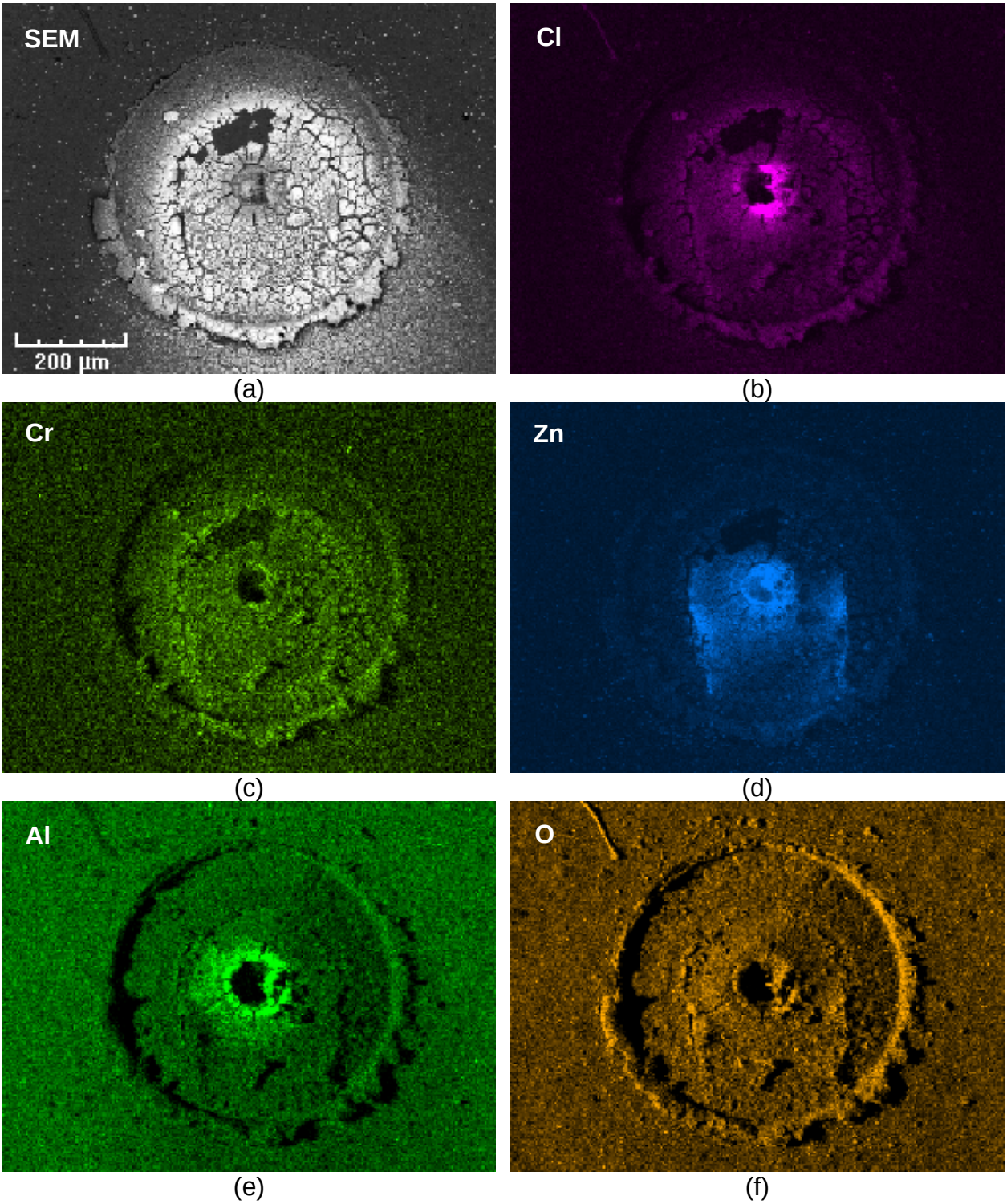

Figure 12: SEM micrograph (a) and EDX element-distribution maps (b-f) displaying the corrosion products precipitated within the circular hole operated in the coil-coated sample. The analysed elements are indicated in the corresponding graphs.